Real-Time Transient Instability Detection in the Power System With High DFIG-Wind Turbine Penetration via Transient Energy

Shabani, Hamid Reza; Kalantar, Mohsen; Hajizadeh, Amin

Published in:
I E E E Systems Journal

DOI (link to publication from Publisher):
10.1109/JSYST.2021.3079253

Publication date:
2022

Document Version
Accepted author manuscript, peer reviewed version

Real-Time Transient Instability Detection in the Power System With High DFIG-Wind Turbine Penetration via Transient Energy

Hamid Reza Shabani, Mohsen Kalantar, *Member, IEEE*, and Amin Hajizadeh, *Senior Member, IEEE*

***Abstract*—By increasing the penetration of wind power in the modern power systems, to investigate transient stability is of special importance. This article presents an innovative index based on the concept of the potential energy boundary surface along with kinetic energy, which aims to detect the transient instability of a power system comprising doubly fed induction generator (DFIG)-based wind farms. Accordingly, transient instability detection (TID) is performed without directly calculating the unstable equilibrium point and thus the computational load is decreased. Since the proposed approach requires only the postfault data that can be easily measured by the phasor measurement units, it is suitable for real-time applications. Therefore, the proposed approach can be applied as a general tool to any power system with any change in topology and operating conditions. Moreover, considering that the current-balance form is the preferred industry model for the implementation of transient stability simulation, the network equations in the current-balance form are extracted for grid-connected DFIG and synchronous generators. Different scenarios are simulated in the Western System Coordinating Council 3-machine, 9-bus system, and the 10-generator New England system. To validate the new index for TID, simulation results are compared with the transient stability index and out-of-step distance relay. The obtained results validate the correctness and effectiveness of the presented new index.**

***Index Terms*—Kinetic energy (KE), potential energy boundary surface (PEBS), transient energy function (TEF), transient instability detection (TID), wind farm.**

NOMENCLATURE

Abbreviations

DFIG	Doubly fed induction generator.
TID	Transient instability detection.
CCT	Critical clearing time.
SG	Synchronous generator.
T-D	Time-domain.
TEF	Transient energy function.
UEP	Unstable equilibrium point.
SEP	Stable equilibrium point.
SNR	Signal-to-noise ratio.
KE	Kinetic energy.
PE	Potential energy.
SI	Simultaneous implicit.
TSA	Transient stability assessment.
DAE	Differential-algebraic equation.
PEBS	Potential energy boundary surface.
NPI	New PEBS-based index.
RSC	Rotor side converter.
GSC	Grid side converter.
NAE	Nonlinear algebraic equations.
NDE	Nonlinear differential equations.
TSI	Transient stability index.
OOS	Out-of-step.
PMU	Phasor measurement unit.

Parameters and Variables

η	TSI symbol.
$\rho_{\max}$	Maximum angle separation.
T'_{d0}	d-axis open circuit time constant.
T'_{q0}	q-axis open circuit time constant.
E'_d	d-axis transient voltage of SG.
E'_q	q-axis transient voltage of SG.
X_d	d-axis synchronous reactance.
X_q	q-axis synchronous reactance.
X'_d	d-axis transient reactance.
X'_q	q-axis transient reactance.
I_d	d-axis current of SG.
I_q	q-axis current of SG.
E_{fd}	Voltage applied to the SG field winding.
δ	Rotor angle.
ω	Rotor velocity of SG.
ω_s	Synchronous speed.
M	Inertia constant of SG.
T_M	Mechanical torque of SG.
T_E	Electromagnetic torque of SG.
T_A	Exciter time constant.
V_{ref}	Reference voltage of the excitation system.
K_A	Gain of excitation system.
V_t	Magnitude of terminal voltage.
θ_t	Angle of terminal voltage.
P_{tw}	Extracted wind turbine power.
ρ	Air density.
R	Blade length.

Manuscript received November 28, 2020; revised March 19, 2021; accepted May 4, 2021. *(Corresponding author: Mohsen Kalantar.)*

Hamid Reza Shabani and Mohsen Kalantar are with the Center of Excellence for Power System Automation and Operation, Department of Electrical Engineering, Iran University of Science and Technology, Tehran 1684613114, Iran (e-mail: h_shabani@elec.iust.ac.ir; kalantar@iust.ac.ir).

Amin Hajizadeh is with the Department of Energy Technology, Aalborg University, 6700 Esbjerg, Denmark (e-mail: aha@et.aau.dk).

Digital Object Identifier 10.1109/JSYST.2021.3079253

C_p	Performance coefficient.
λ	Tip speed ratio.
β	Blade pitch angle.
V_w	Wind speed.
ω_t	Wind turbine speed.
ω_{elB}	Electrical base speed.
ω_r	Rotor speed of DFIG.
t_{cl}	Fault clearing time.
D	Damping term of SG.
I_{qtD}	q-axis total output current of DFIG.
I_{dtD}	d-axis total output current of DFIG.
$I_{\rm GSC}$	Current of grid-side convertor.
α	Reactive power sharing between stator and grid-side convertor.
Q_s	Stator reactive power of DFIG.
$Q_{\rm tot}$	Total reactive power of DFIG.
$Q_{\rm GSC}$	Reactive power of grid-side convertor.
P_r	Rotor active power of DFIG.
$P_{\rm GSC}$	Active power of grid-side convertor.
θ_{tD}	Angle of DFIG terminal voltage.
V_{tD}	Magnitude of DFIG terminal voltage.
C	Drive-train damping coefficient.
K	Drive-train shaft stiffness.
θ_{tw}	Twist angle of drive-train shaft.
$T_{\rm sh}$	Shaft torque.
T_e	Electrical torque of wind turbine.
T_t	Mechanical torque of wind turbine.
H_g	Generator inertia of DFIG.
H_t	Wind turbine inertia.
L_{ss}	Stator inductance of DFIG.
L_{rr}	Rotor inductance of DFIG.
L_m	Mutual inductance of DFIG.
r_s	Stator resistance of DFIG.
r_r	Rotor resistance of DFIG.
V_{ds}	d-axis stator voltage of DFIG.
V_{qs}	q-axis stator voltage of DFIG.
V_{dr}	d-axis rotor voltage of DFIG.
V_{qr}	q-axis rotor voltage of DFIG.
e'_q	q-axis internal voltage of DFIG.
e'_d	d-axis internal voltage of DFIG.
i_{ds}	d-axis stator current of DFIG.
i_{qs}	q-axis stator current of DFIG.
δ_i^s	Stable equilibrium points for postfault system.
k	Number of machines (SGs and DFIGs).
$Y'_{ij}e^{j\alpha'_{ij}}$	Reduced network-admittance matrix.

I. Introduction

In RECENT years, renewable energies and their integration into the power systems have gained significant global attention. Meanwhile, power generation from wind energy is one of the leading technologies in renewable energy alternatives. According to the latest report of the Global Wind Energy Council, wind energy capacity installed globally was equal to 60.4 GW in 2019. Also, 2020 was a record year for wind power growth in both North and Latin America, with nearly 22 GW of capacity installed despite COVID-19 impacts, demonstrating the incredible resilience of the wind industry and solidifying its crucial role in the region [1]. With the high penetration of wind power, one of the most important challenges facing the power system is the transient stability analysis [2]. Therefore, in this article, the transient stability of modern power systems is discussed. To do this, an aggregated model of doubly fed induction generator (DFIG)-based wind farm is used that it is integrated into the power system.

Transient stability is concerned with the ability of the power system to maintain synchronism when subjected to a severe disturbance [3]. Traditionally, transient stability assesses with monitoring of the speed and rotor angle of the synchronous generators (SGs) [4]. Also, transient stability study is generally of two types: evaluation and detection or prediction [3], [5]. In transient stability evaluation, the critical clearing time (CCT) is a very important parameter and is defined as the maximal fault duration for which the system remains transiently stable [3], [6]. But for transient instability detection (TID), the CCT is not of interest. In this aspect, the aim is to monitor the transient behavior of the power system when a disturbance occurs [3], [7]. The important point in this field is that fast prediction or detection of transient stability makes it possible to take emergency control measures efficiently.

A considerable literature has been conducted on TID of the traditional power systems under various conditions in the presence of SGs [8]–[11]. Time-domain (T-D) simulation and transient energy function (TEF) methods are playing a more important role in TID [5]. In the work [8], a new criterion is proposed to quickly evaluate the online TID based on the TEF method. Study [9] proposes a novel self-tuning algorithm that estimates the generator instability. The proposed algorithm uses the unstable equilibrium point (UEP) that is estimated by the least-squares curve fitting technique on the power-angle plane. In [8] and [9], classical model (simplified model) has been used for SGs. The proposed approach in [10] is based on the corrected kinetic energy (KE) and also a new concept of the equal area that calculates UEP, which is applied for estimating CCT. In [11], TEF and the maximum potential energy (PE) are used to evaluate critical energy for TID. One of the most important issues that limit the use of TEF methods for TID is the need to calculate directly the UEP or the value of critical energy, which results in a large computational load [12]. Also, today intelligent methods based on fuzzy systems, neural networks, and pattern recognition algorithms are used more frequently for real-time TID [5], [7]. However, all of these methods are highly dependent on power system parameters and are not a general tool to be used in all grids with different parameters [13]. As mentioned above, the literature on TID methods has some defects and limitations.

When wind power penetration in the power system is low, wind turbines do not mainly interfere with voltage and frequency control and are disconnected from the grid in the event of the fault [14]. However, as the penetration of wind farms is high, it seems necessary to study their impact on the dynamic behavior of the modern power system. One of the first studies conducted in this field aimed to show the impact of the integration of a wind power plant on the oscillation damping caused by a disturbance [15]. Also, the work [16] investigates the impact

of power system strength and phase-locked loop parameters on the stability of grid-connected DFIG-based wind farms. Some other types of research conducted in this field have focused on how to model and provide an equivalent circuit of DFIG for the dynamic studies in the power systems. The study in [17] provides a suitable model to study the transient stability of DFIG and uses the simultaneous implicit (SI) method for T-D simulation. Other studies have compared the impact of different types of wind turbine generators on evaluating the transient stability of the power system [18], [19]. In these studies, a new quantitative transient stability assessment (TSA) is conducted using the transient energy margin based on TEF for a power system with a high penetration of DFIG-based wind farms. In [20], the impact of high penetration of wind power on the transient stability of a multimachine system is discussed and a new index based on DFIG terminal voltage sensitivity is proposed to evaluate the transient stability margin. The work in [21] also presents a novel approach for real-time TSA based on corrected KE, which aims to assess transient stability by calculating the CCT in a power system consisting of wind turbines. Considering the studies reviewed above, it can be observed that a small number of the works have presented new indexes for real-time TID in the power systems with the high penetration of DFIG-based wind farms.

In this article, a new approach is presented for real-time TID and is investigated for traditional and modern power systems. To do this, the SI method is used for T-D simulation. At first, the differential-algebraic equation (DAE) model with the network equations in the current-balance form is extracted for grid-connected DFIG and SGs. The current-balance form is the preferred industry model since the network-admittance matrix has to be refactored only when a disturbance is occurring [22]. In this way, transient stability simulation is simplified and computational load is decreased. Actually, using the concept of the potential energy boundary surface (PEBS) along with KE, the new PEBS-based index (NPI) for TID is presented. Despite using the concepts of the TEF and the characteristics of the UEP in this article, there is no need to directly calculate the UEP. Therefore, the computational load is greatly decreased and can be suitable for real-time applications. To validate the new approach for TID, different scenarios are simulated in the Western System Coordinating Council (WSCC) 3-machine, 9-bus system, and the 10-generator New England system. The obtained results approve the efficiency of the proposed approach.

II. Model of the Power System

A. Modeling of the SG

In a power system with m machines, the equations of the two-axis model of the SG with a static excitation system can be defined as follows [22]:

$$T'_{d0i}\frac{d}{dt}E'_{qi} = -E'_{qi} - (X_{di} - X'_{di})\,I_{di} + E_{fdi} \tag{1}$$

$$T'_{q0i}\frac{d}{dt}E'_{di} = -E'_{di} + \left(X_{qi} - X'_{qi}\right)I_{qi} \tag{2}$$

$$\frac{d}{dt}\delta_i = \omega_i - \omega_s \tag{3}$$

$$M_i\frac{d}{dt}\omega_i = T_{Mi} - T_{Ei} - D_i\left(\omega_i - \omega_s\right) = f_i(\delta) \tag{4}$$

$$T_{Ai}\frac{d}{dt}E_{fdi} = -E_{fdi} + K_{Ai}\left(V_{\mathrm{ref}i} - V_{ti}\right) \tag{5}$$

$$E'_{di} - V_{ti}\sin\left(\delta_i - \theta_{ti}\right) - R_{si}I_{di} + X'_{qi}\,I_{qi} = 0 \tag{6}$$

$$E'_{qi} - V_{ti}\cos\left(\delta_i - \theta_{ti}\right) - R_{si}I_{qi} - X'_{di}\,I_{di} = 0 \tag{7}$$

where

$$T_{Ei} = \left[E'_{di}I_{di} + E'_{qi}I_{qi} + \left(X'_{qi} - X'_{di}\right)I_{di}I_{qi}\right] \quad i = 1, 2, \ldots, m. \tag{8}$$

B. Modeling of the DFIG-Based Wind Turbine

In power system stability studies, a static model is typically used for the aerodynamic system of the turbine [18]

$$P_{tw} = (0.5)\ \rho\pi R^2 C_p\left(\lambda, \beta\right)V_w^3\,. \tag{9}$$

Also, the drive-train system is represented by the two-mass model [23] as shown in the following:

$$\frac{d}{dt}\omega_t = \frac{1}{2H_t}\ \left(T_t - T_{\mathrm{sh}}\right) \tag{10}$$

$$\frac{d}{dt}\omega_r = \frac{1}{2H_g}\ \left(T_{\mathrm{sh}} - T_e\right) \tag{11}$$

$$\frac{d}{dt}\theta_{tw} = \omega_{elB}\ \left(\omega_t - \omega_r\right) \tag{12}$$

$$T_{\mathrm{sh}} = K\theta_{tw} + C\frac{d}{dt}\theta_{tw}. \tag{13}$$

The dynamic equations of the DFIG in the synchronous reference frame as a voltage source behind a transient reactance can be represented as (14)–(18) [23]

$$\frac{L'_s}{\omega_{elB}}\frac{di_{qs}}{dt} = -R_1 i_{qs} - \omega_s L'_s i_{ds} + k_{mrr}V_{qr} + \frac{1}{T_r\omega_s}e'_d - V_{qs} + \left(\frac{\omega_r}{\omega_s}\right)e'_q \tag{14}$$

$$\frac{L'_s}{\omega_{elB}}\frac{di_{ds}}{dt} = -R_1 i_{ds} + \omega_s L'_s i_{qs} + k_{mrr}V_{dr} - \frac{1}{T_r\omega_s}e'_q - V_{ds} + \left(\frac{\omega_r}{\omega_s}\right)e'_d \tag{15}$$

$$\frac{1}{\omega_s\omega_{elB}}\frac{de'_d}{dt} = R_2\, i_{qs} - \frac{1}{T_r\omega_s}e'_d + \left(1 - \frac{\omega_r}{\omega_s}\right)e'_q - k_{mrr}V_{qr} \tag{16}$$

$$\frac{1}{\omega_s\omega_{elB}}\frac{de'_q}{dt} = -R_2 i_{ds} - \frac{1}{T_r\omega_s}e'_q - \left(1 - \frac{\omega_r}{\omega_s}\right)e'_d + k_{mrr}V_{dr} \tag{17}$$

where

$$T_e = e'_d i_{ds} + e'_q i_{qs} \tag{18}$$

$$k_{mrr} = \frac{L_m}{L_{rr}};\ L'_s = L_{ss} - \frac{L_m^2}{L_{rr}};\ T_r = \frac{L_{rr}}{r_r};\ R_2 = k_{mrr}^2\, r_r$$

$$R_1 = r_s + R_2;\ e'_q = k_{mrr}\,\omega_s \lambda_{dr};\ e'_d = -k_{mrr}\omega_s \lambda_{qr}.$$

The equations of the DFIG exact model are not suitable for transient stability studies because the interface with the grid voltage and current phasors is not easy to implement in this case [14], [17]. Accordingly, in this article, stator transients in the DFIG dynamic model are ignored ($\frac{di_{qs}}{dt} = \frac{di_{ds}}{dt} = 0$). Additionally, since the current controllers on power electronic converters are much faster than the studied electromechanical transients, they do not have a significant impact on the transient stability of the power system [14]. Accordingly, the converters are considered ideal and the rotor side converter (RSC) is modeled as the voltage source and the grid side converter (GSC) as the current source. Also, the classical vector control method [24] is applied and the wind farm is represented by an aggregated model.

C. External Grid

The power system is represented by a set of nonlinear algebraic equations (NAEs) in two classifications: the NAEs in power-balance and current-balance form. For the NAEs in power-balance form, the Jacobian of the network equations contains the power flow Jacobian, and thus it is useful in small-signal analysis and voltage collapse studies. On the other hand, for the NAEs in current-balance form, since the network-admittance matrix has to be refactored only when a disturbance is occurring, it is the preferred industry model and, in this way, transient stability simulation is simplified [22]. Accordingly, the NAEs in the current-balance form are extracted for the grid-connected DFIG and SG. In this way, there are only injected currents at the generator buses and thus the load buses can be eliminated from the network equations. Also, the loads are assumed to be constant impedance models. This model is widely used in first-swing transient stability analysis [8], [22]. Accordingly, the complex NAEs in current-balance form for the reduced-order model of the power system is shown as follows:

$$(I_{di} + jI_{qi})\ e^{j\left(\delta_i - \frac{\pi}{2}\right)} = \sum_{k=1}^{m} \left[Y'_{ik} e^{j\alpha'_{ik}}][V_{tk} e^{j\theta_{tk}}\right]. \tag{19}$$

By simplifying (19), the NAEs in current-balance form can be obtained for SG as follows:

$$[I_{di}\sin(\delta_i) + I_{qi}\cos(\delta_i)] = \sum_{k=1}^{m} [V_{tk}G'_{ik}\cos(\theta_{tk}) - V_{tk}B'_{ik}\sin(\theta_{tk})] \tag{20}$$

$$[I_{qi}\sin(\delta_i) - I_{di}\cos(\delta_i)] = \sum_{k=1}^{m} [V_{tk}G'_{ik}\sin(\theta_{tk}) + V_{tk}B'_{ik}\cos(\theta_{tk})]. \tag{21}$$

Similarly, the NAEs in the current-balance form can be obtained for DFIG. To exchange power between the DFIG and the power system, it is necessary to determine the interface between DFIG and the grid. The equation of the terminal voltage of DFIG can be expressed in terms of the common reference frame as follows:

$$V_{tD}\, e^{j\theta_{tD}} = (V_{ds} + jV_{qs})\, e^{j\left(\delta - \frac{\pi}{2}\right)}. \tag{22}$$

According to the classical vector control method, the active and reactive powers of the stator are controlled independently in DFIG using the q-axis and d-axis currents, respectively [24]. Since the stator flux vector is aligned with the d-axis of the synchronous reference frame, the terminal voltage vector is aligned with the q-axis of the machine. Thus, ($V_{ds} = 0,\ V_{qs} = V_{tD}$ and $\theta_{tD} = \delta$). On the other hand, the GSC is modeled as a current source and it is assumed that the reactive power is exchanged with the grid only by the DFIG stator

$$P_{\rm GSC} = P_r = (V_{qr}\, i_{qr} + V_{dr} i_{dr});\ Q_{\rm GSC} = \alpha Q_{\rm tot}$$

$$\alpha = 0 \Rightarrow Q_{\rm GSC} = 0 \Rightarrow Q_s = (1-\alpha)\, Q_{\rm tot} = Q_{\rm tot}.$$

Therefore, the current of the GSC can be expressed as follows:

$$I_{\rm GSC} = \frac{P_{\rm GSC} - jQ_{\rm GSC}}{-jV_{qs}} = j\frac{P_r}{V_{qs}}. \tag{23}$$

According to the above-mentioned points, injected current to the grid at the DFIG bus is obtained as follows:

$$(I_{dtD} + jI_{qtD}) = \left(i_{ds} + j\left(i_{qs} + \frac{P_r}{V_{qs}}\right)\right). \tag{24}$$

Hence, by combining (19) and (24), the complex NAEs in current-balance form for DFIG can be obtained as follows:

$$(I_{dtD} + jI_{qtD})\ e^{j\left(\theta_{tD} - \frac{\pi}{2}\right)} = \sum_{k=1}^{m} \left[Y'_{ik} e^{j\alpha'_{ik}}][V_{tk} e^{j\theta_{tk}}\right]. \tag{25}$$

By simplifying (25), the NAEs in current-balance form can be rewritten as (26) and (27)

$$\left[i_{ds}\sin(\theta_{tD}) + ((i_{qs} + \frac{P_r}{V_{qs}})\cos(\theta_{tD}))\right] = \sum_{k=1}^{m} [V_{tk}G'_{ik}\cos(\theta_{tk}) - V_{tk}B'_{ik}\sin(\theta_{tk})] \tag{26}$$

$$\left[((i_{qs} + \frac{P_r}{V_{qs}})\sin(\theta_{tD})) - i_{ds}\cos(\theta_{tD})\right] = \sum_{k=1}^{m} [V_{tk}G'_{ik}\sin(\theta_{tk}) + V_{tk}B'_{ik}\cos(\theta_{tk})]. \tag{27}$$

III. TSA Using T-D Simulation

According to Section II, the dynamic modeling of the power system can be represented using a set of DAEs. When analyzing the transient stability using the T-D simulation, the DAEs should be solved step by step in the time domain. One of the most effective methods for this purpose is the SI method [22]. In this

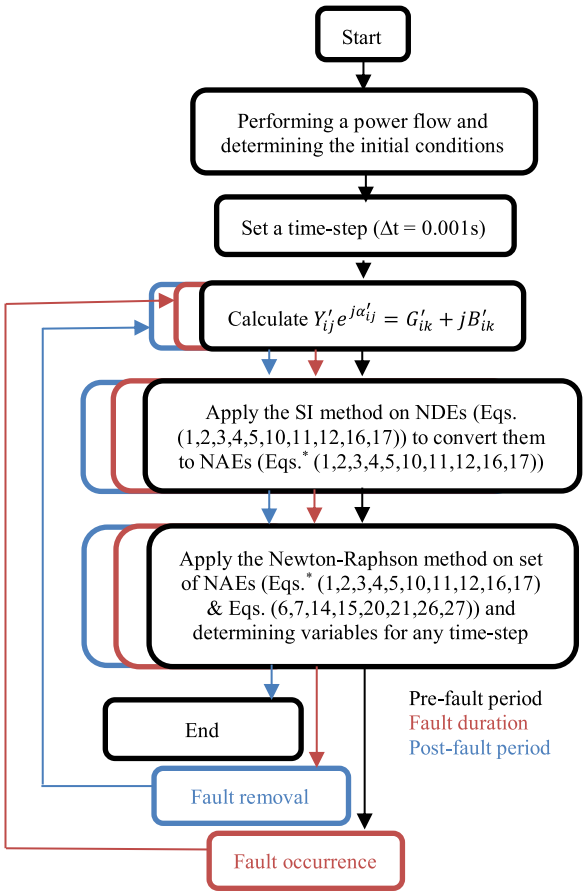

Fig. 1. Flowchart of the T-D simulation.

method, using trapezoidal numerical integration at any time step, nonlinear differential equations (NDEs) are converted to NAEs, and the set of equations is solved using the Newton–Raphson method. A flowchart addressing the step-by-step procedure of the T-D simulation is shown in Fig. 1. Calculating the initial conditions of the system variables is the first step for transient stability studies that are obtained by load flow. The DFIG is considered as a PQ bus because it works at a specified power factor (this case is in most applications [17]). Then, by adjusting the time step, the T-D simulation is started. As can be observed that in any three study periods (prefault, fault, and postfault), the simulation process is the same, and only when a disturbance is occurring or is removed, $Y'_{ij}e^{j\alpha'_{ij}}$ has to be refactored.

IV. Proposed Approach for TID

A. Concept of Transient Energy and PEBS

Whenever a fault occurs in a power system, there is some extra energy at the moment of clearing the fault that should be absorbed by the grid to keep the power system stable. This energy is called transient energy. Transient energy is the extra KE injected into the power system during a fault. The ability of the grid to absorb the extra energy depends largely on its ability to convert this energy into PE, and this, in turn, depends on the structure of the power system after clearing the fault.

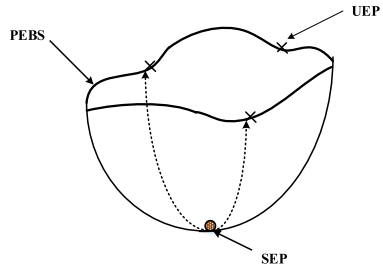

Fig. 2. PE well.

For a given structure of the power system, there is a critical or maximum value of transient energy that the system can absorb or convert into other forms of energy. If the extra transient energy injected into the system at the moment of clearing the fault is less than the value of critical energy, the machine rotor will oscillate and extra energy will be absorbed by the system, in which case the system is stable [8], [22]. This can be explained using the concept of the PE well, which is shown in Fig. 2.

A ball is shown inside the PE well that indicates a stable equilibrium point (SEP) of the steady-state of the system. The edges of the PE well include several saddle points and extremum points, which are called UEPs. These points are connected at the edges of the PE well by the PEBS [22].

B. Proposed Approach

The sum of the KE and PE is equal to TEF and it is considered for the postfault system. The KE is defined as follows [22]:

$$V_{\mathrm{KE}} = \sum_{i=1}^{m} \frac{1}{2} M_i (\omega_i - \omega_s)^2. \tag{28}$$

Thus, the derivative of the KE is obtained as follows:

$$\frac{dV_{\mathrm{KE}}}{dt} = \sum_{i=1}^{m} M_i \frac{d\omega_i}{dt} (\omega_i - \omega_s). \tag{29}$$

According to (4), (29) can be written as follows:

$$\frac{dV_{\mathrm{KE}}}{dt} = \sum_{i=1}^{m} f_i(\delta) [\omega_i - \omega_s]. \tag{30}$$

TEF remains constant with the fault clearance if the system is assumed to be conservative [22]

$$\frac{dV_{\mathrm{PE}}}{dt} + \frac{dV_{\mathrm{KE}}}{dt} = 0. \tag{31}$$

Accordingly, the first important point is that the peak PE and minimum KE occur at the same time [8], [22]. Therefore, instead of calculating the value of the critical energy that is equal to the peak PE, the minimum KE can be calculated. In the stable condition, all of the KE injected into the system is converted into PE and nothing remains. Thus, the value of minimum KE is close to zero. However, the value of KE in this state is not exactly equal to zero [8]. On the other hand, in the unstable condition, the trajectory of the system crosses the PEBS at a UEP and the minimum value of KE is such that a part of it is not absorbed by the system after clearing the fault. As a result,

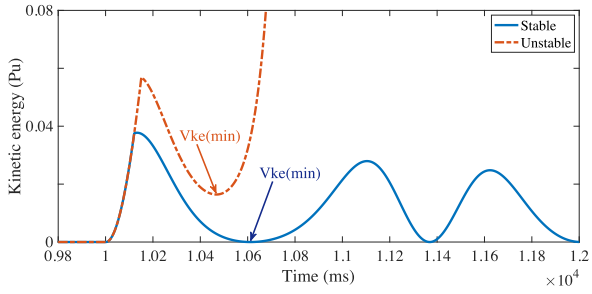

Fig. 3. Curve of KE for the stable and unstable condition.

the minimum KE is increased and is nonzero in this state [8], [22]. This has been shown in Fig. 3 by simulation. Therefore, the second important point is that in the unstable condition, the trajectory of the system crosses the PEBS at a UEP and the KE is minimum at this moment.

According to (30) and (31) and combined with (3), the derivative of the PE is obtained as follows:

$$\frac{dV_{\mathrm{PE}}}{dt} = -\sum_{i=1}^{m} f_i(\delta)\left[\frac{d\delta_i}{dt}\right]. \tag{32}$$

By simplifying (32), the expression of PE is obtained as follows:

$$\frac{dV_{\mathrm{PE}}}{d\delta} = -\sum_{i=1}^{m} f_i(\delta). \tag{33}$$

According to (33), the PEBS function is also defined as follows [22]:

$$\text{PEBS function} = \sum_{i=1}^{m} f_i(\delta)\left[\delta_i - \delta_i^s\right]. \tag{34}$$

Whenever the PEBS function is equal to zero, it means that the trajectory of the system has crossed the PEBS. Accordingly, when the sign of the PEBS function is changed from negative to positive, the power system is unstable [22]. Also, as can be observed, $\frac{dV_{\mathrm{KE}}}{dt}$, $\frac{dV_{\mathrm{PE}}}{dt}$, and PEBS function are proportional to $f_i(\delta)$. Thus, when the trajectory of the system crosses the PEBS and (34) is equal to zero, the derivative of the KE and PE is equal to zero according to (30) and (32). Therefore, the PE is maximum and the KE is minimum at this moment.

Thus, according to what is said above, the following three important points for the unstable conditions can be expressed.

1) The system trajectory crosses the PEBS at an UEP.
2) KE is minimum at the UEP. Therefore, due to being conservative, the value of PE is maximum and equal to the critical energy at this moment.
3) The PEBS function changes from negative to positive.

It is clear that the UEP plays an important role in TID. However, the computational load and complexity of calculating the UEP, especially in multimachine power systems, is one of the most important problems in this field. The main idea in this article is TID without directly calculating the UEP. In the new proposed approach, the stable and unstable conditions are identified according to the characteristics of the UEP and the behavior of KE and the PEBS function. In fact, after clearing the fault, if the system trajectory reaches the UEP and crosses the PEBS, the system will be unstable so that the KE is minimum and the sign of the PEBS function changes from negative to positive at that moment. Accordingly, the proposed NPI for TID can be represented as follows:

$$\text{NPI} = \left\{ \begin{array}{c} \text{Stable, If for } t > t_{cl} : \\ V_{\mathrm{KE}} = V_{\mathrm{KE(min)}} \approx 0 \quad \text{PEBS function} < 0, \neq V_{\mathrm{KE(min)}} \\ \text{Unstable, If for } t > t_{cl} \\ V_{\mathrm{KE}} = V_{\mathrm{KE(min)}} > 0 \quad \text{PEBS function} > 0, = V_{\mathrm{KE(min)}} \end{array} \right\}.$$

KE is always positive and the PEBS function is negative in the stable condition [22]. Therefore, if the curves of the KE and the PEBS function are monitored for the duration of the postfault system, the two curves will not intersect when the system is stable. However, if the system is unstable, especially in the case of the transient instability of the first-swing, on the one hand, the PEBS function must change the sign to exceed zero and become positive, and on the other hand, KE is minimum and nonzero at this moment. In other words, in the unstable condition, the moment when the PEBS function is to exceed zero and change the sign is exactly the moment when the KE curve is nonzero and has a minimum value. Therefore, according to the NPI, an important index for detecting definitely instability is that the curve of the PEBS function that is on the negative side and close to zero crosses the curve of the KE that is on the positive side and significantly increases. In such a condition, one can be sure that the PEBS function is positive and the system is unstable. Therefore, using the NPI for TID, it is necessary to measure the rotor angle, velocity, and output power of the generator to monitor the PEBS function and KE immediately after clearing the fault.

V. Numerical Simulation Results and Discussion

The WSCC 3-machine, 9-bus system [22], and the 10-generator New England system [18] are utilized to verify the effectiveness and correctness of the proposed approach. All of the numerical simulations are conducted on MATLAB environment and the sampling rate for calculation of the variables is chosen 1 ms ($\Delta t = 0.001$ s).

A. WSCC 3-Machine, 9-Bus System Case Study

In this section, the WSCC 3-machine, 9-bus system is used as a test power system for validation of the proposed approach. Also, to evaluate the proposed approach for transient stability of the modern power system, an aggregated model of DFIG-based wind farm is integrated to the test power system. According to the power system modeling in Section II, transient stability studies are performed using T-D simulation by the SI method. The time response of the system dynamics is simulated to be 10 s in the operating conditions of the steady-state and then the fault occurs. The fault type is a three-phase short circuit and is occurring in all buses. For generation buses, the fault is cleared without removing the line and for other buses, it is cleared by removing a line. Actually, an N-1 contingency level [25] is considered. The

TABLE I
UNDER STUDY SCENARIOS

Scenarios	Factors	Details description	
Scenario 1	Base Case	There isn't DFIG integrated into the grid Total active power of the SGs 319.6MW	
Scenario 2	DFIG Capacity	Case A	100MW DFIG integrated at bus 7
		Case B	200MW DFIG integrated at bus 7
Scenario 3	DFIG Location	Case A	100MW DFIG integrated at bus 9
		Case B	100MW DFIG integrated at bus 4

TABLE II
COMPARISON OF THE NPI WITH TSI AND OOS FOR TID

Faulted bus (line tripped)	CCT (s)	Instability detection time (s)		
		TSI	OOS	NPI
4(4-6)	0.269-0.270	11.006	10.700	10.500
5(5-7)	0.244-0.245	18.720	18.468	18.308
6(6-9)	0.334-0.335	13.624	13.385	13.140
7(7-5)	0.132-0.133	18.663	18.421	18.170
8(8-7)	0.259-0.260	11.228	11.044	10.857
9(9-8)	0.221-0.222	10.833	10.664	10.572
1(-)	0.307-0.308	11.003	10.808	10.656
2(-)	0.214-0.215	11.119	10.930	10.664
3(-)	0.251-0.252	11.000	10.757	10.602

indexes of CCT, transient stability index (TSI), and out-of-step (OOS) are considered for comparative studies. TSI is defined in (35) [26]. The power system is considered stable if the value of η is greater than zero

$$\eta = \frac{360 - \rho_{\max}}{360 + \rho_{\max}} \times 100. \tag{35}$$

Also, the OOS criterion is the rotor angle exceeding 180 degrees and it is based on OOS distance relay operation [4]. Accordingly, the factors considered for the investigation of the effectiveness of the proposed approach are listed in Table I.

1) Scenario 1: In this section, the base case of the WSCC 3-machine, 9-bus system is used to evaluate the effectiveness of the NPI for TID. To do this, the N-1 contingency level is applied and the CCT is calculated using the T-D simulation for all cases. Then, for any cases, the fault clearing time is set to be equal to the CCT in the unstable condition, and TID is performed using the proposed approach. In this way, the NPI is used for TID and the results obtained are compared with those from TSI and OOS index. Accordingly, the simulation results are listed in Table II. As can be observed, the NPI has been able in all cases to correctly recognize instability in a shorter period than the TSI and OOS. Based on the results, the NPI can detect instability earlier than the TSI and OOS, respectively, by 414.1 and 224.3 ms on average.

Additionally, to demonstrate how operating the proposed approach, for instance, the fault occurrence on bus 8 is considered. According to the CCT in Table II, the system is stable when the fault clearing time is set to be 0.259 s. Thus, the fault is occurring on bus 8 and is cleared at the 0.259 s by removing line 8–7. If the curves of the KE and the PEBS function are monitored for the duration of the postfault system, the two curves will not intersect because the system is stable. This is shown by simulation in Fig. 4.

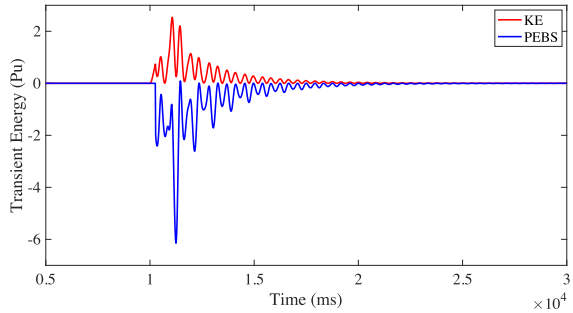

Fig. 4. KE and PEBS function in the stable condition.

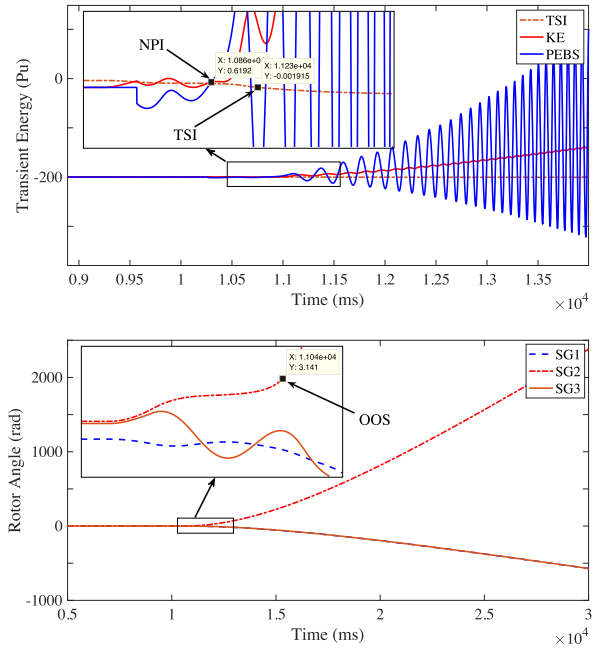

Fig. 5. KE, TSI, PEBS, and rotor angle of SGs in the unstable condition.

For unstable conditions, the T-D simulation is repeated with the fault clearing time is set to be 0.26 s. Fig. 5 shows TID using NPI and its comparison with TSI and OOS.

In unstable conditions, the PEBS function crosses the curve of the KE, and its sign changes from negative to positive and increases. Therefore, using the NPI, the transient instability can be detected correctly and it detects instability earlier than TSI and OOS. In fact, the sooner the transient instability is detected, the more time is left to take corrective and preventive measures to prevent total instability and blackouts in the power system. As a result, the important point that can be said concerning the TID is that in addition to accuracy, instability can be detected earlier by the NPI than the TSI and OOS. Thus, this approach is suitable for real-time applications.

2) Scenario 2: This section generally focuses on the high penetration of DFIG-based wind farms. To investigate the proposed approach for TID of the modern power systems, an aggregated model of DFIG-based wind farm is used for integrating to the test power system. Accordingly, a DFIG-based wind farm is integrated into the test power system in parallel with SG2 at

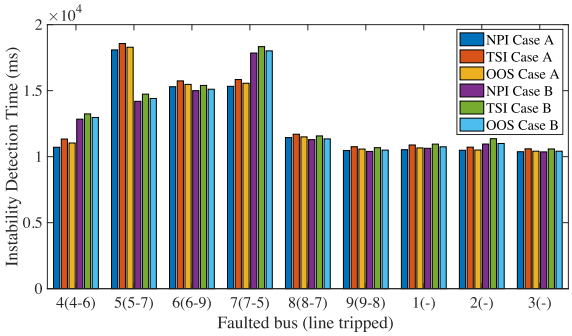

Fig. 6. Comparison of the NPI with TSI and OOS for TID.

TABLE III
COMPARISON OF THE NPI WITH TSI AND OOS FOR TID

Faulted bus (line tripped)	Instability detection time (s)					
	Case A			Case B		
	NPI	TSI	OOS	NPI	TSI	OOS
4(4-6)	10.579	11.048	10.768	10.443	10.872	10.588
5(5-7)	15.397	15.965	15.658	13.364	13.800	13.559
6(6-9)	12.754	13.405	13.155	10.640	11.209	10.954
7(7-5)	15.336	15.842	15.539	11.892	12.457	12.225
8(8-7)	10.490	10.882	10.692	10.787	11.136	10.945
9(9-8)	10.604	10.999	10.780	10.395	10.639	10.456
1(-)	10.709	11.041	10.871	10.537	10.955	10.701
2(-)	10.385	10.689	10.496	10.438	10.825	10.586
3(-)	11.005	11.236	11.088	10.402	10.793	10.639

bus 7. (It does not replace SG2.) In Case A, the capacity of the DFIG-based wind farm is set to be 100 MW (constructed from 20 individual units with a nominal capacity 5 MW [27]). Here, it is assumed that the generated power from the DFIG-based wind farm is 63 MW, which is accounted for 20% of the total consumed power of the test power system. Also, the penetration of wind power is increased to 40% by increasing the capacity of a DFIG-based wind farm to 200 MW in Case B. The conditions of the fault occurrence are the same as in the previous section. Here too, for all of the cases, the fault clearing time is set to equal to the CCT in the unstable condition, and the NPI is used for TID. In this way, T-D simulation based on the proposed approach is performed and the simulation results are shown in Fig. 6.

The situation is the same in this scenario and the NPI has a significant performance for TID. In Case A, the NPI can detect instability earlier than the TSI and OOS, respectively, by 354.4 and 151.1 ms on average and for Case B, these values are equal to 385.3 and 135.2 ms, respectively.

3) Scenario 3: Finally, in scenario 3, the influence of different access locations of the integrated DFIG-based wind farm on TID using NPI is investigated. Accordingly, in Cases A and B, a 100-MW DFIG-based wind farm is integrated at bus 9 and bus 4, respectively, with no SG replaced. It is assumed here that the generated power from the DFIG-based wind farm is accounted for 20% of the total consumed power of the test power system. Also, the conditions of the fault occurrence are the same as in the previous sections. T-D simulation is performed and NPI is used for TID. The simulation results and comparison with TSI and OOS for all cases are listed in Table III.

TABLE IV
COMPARISON OF THE NPI WITH TSI AND OOS IN WIND OPERATION

Faulted bus (line tripped)	CCT (s)	Instability detection time (s)		
		TSI	OOS	NPI
2(-)	0.083-0.084	15.209	14.790	13.872
3(-)	0.086-0.087	13.570	13.148	11.420
6(6-7)	0.103-0.104	18.324	17.913	16.162
7(7-8)	0.132-0.133	19.510	19.093	17.313
9(9-8)	0.099-0.100	19.688	19.292	16.812
10(10-13)	0.115-0.116	19.557	19.143	17.547
11(11-12)	0.123-0.124	19.777	19.358	17.346
12(12-13)	0.244-0.245	13.790	13.384	11.831
13(13-14)	0.116-0.117	19.902	19.489	17.695
14(14-15)	0.102-0.103	19.857	19.440	17.699
15(15-16)	0.084-0.085	14.558	14.136	12.964
22(22-23)	0.100-0.101	19.618	19.206	17.189
34(-)	0.125-0.126	19.868	19.453	17.064
35(-)	0.127-0.128	13.706	13.312	11.732
36(-)	0.144-0.145	17.930	17.522	15.801
37(-)	0.125-0.126	16.014	15.602	14.009
38(-)	0.085-0.086	12.551	12.209	11.478

As can be observed, the TSI and OOS need more time to detect instability after clearing the fault in all cases. Therefore, in Case A, NPI detects transient instability earlier than TSI by 429.5 ms on average, and OOS by 198.6 ms on average. Also, these values for Case B are 432 and 195 ms, respectively. So here too, the effectiveness of NPI for TID in a shorter time is approved.

B. 10-Generator New England System Case Study

In this section, for more validation of the NPI, the 10-generator New England system is also used for TID. When all the SGs are used in the test power system, it is referred to as "base case." Moreover, to investigate the proposed approach for TID of the modern power systems, SG10 is replaced with an aggregated model of DFIG-based wind farm with the same capacity that it is referred to as "wind operation." Unlike the previous section, here an aggregated model of DFIG-based wind farm is considered as replacing SG10. (It does not parallel with SG10.) After the simulation in the steady-state conditions, the time of the fault occurrence is set equal to 10 s and the fault type is also considered as three-phase at different buses. In this way, TSA is performed and CCT is estimated for all scenarios. Accordingly, as in the previous section, for any scenarios, the fault clearing time is set to be equal to the CCT in the unstable condition, and TID is performed using the NPI. Then, to show the effectiveness of the proposed approach, the results obtained are compared with the result of a conventional OOS distance relay and TSI. Some chosen scenarios from hundreds of simulations have been presented in Table IV.

As can be observed, the NPI has been able in all scenarios to correctly recognize instability in a shorter period than the TSI and OOS. The NPI can detect instability earlier than the TSI and OOS, respectively, by 2077.2 and 1679.2 ms on average. Additionally, for instance, the fault occurrence on bus 37 is considered. According to Table IV, the system is stable when the fault clearing time is set to be 0.125 s. In this state, if the curves

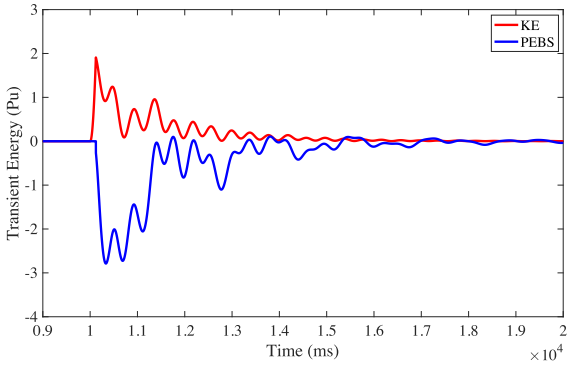

Fig. 7. KE and PEBS function in the stable condition.

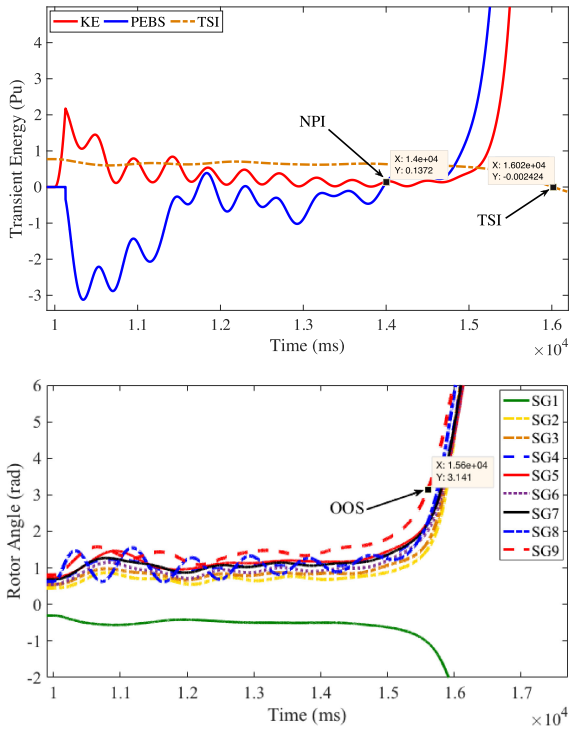

Fig. 8. KE, TSI, PEBS, and rotor angle of SGs in the unstable condition.

of the KE and the PEBS function are monitored for the duration of the postfault system, the two curves will not intersect because the system is stable (see Fig. 7). For unstable conditions, the T-D simulation is repeated with the fault clearing time is set to be 0.126 s. Fig. 8 shows TID using NPI and its comparison with TSI and OOS. Therefore, using the NPI, the transient instability can be detected correctly and it detects instability earlier than TSI and OOS.

1) Impact of Voltage Sag: Generally, voltage sags are the most significant power quality problem faced by industrial customers and large commercial customers. The level of voltage sags at the bus terminal depends on the magnitude and duration of the fault and the sensitivity of the equipment [18]. To investigate the effectiveness of the NPI, simulation is performed for different voltage sag values in two case studies (Base case and Wind operation). For example, simulation results for different voltage sag values are shown for SG8 and DFIG in Table V. As can be observed, the TSI and OOS need more time to detect instability after clearing the fault in all scenarios. Accordingly, in the Base case, NPI detects transient instability earlier than TSI by 996 ms on average, and OOS by 687.4 ms on average. Also, these values for Wind operation are 1843.2 and 1476.2 ms, respectively. So here too, the effectiveness of NPI for TID in a shorter time is approved.

TABLE V
COMPARISON OF THE NPI WITH TSI AND OOS FOR TID

Case studies	Voltage sag (%)	CCT (s)	Instability detection time (s)		
			TSI	OOS	NPI
Base case for SG8	100	0.175-0.176	14.495	14.192	13.508
	80	0.177-0.178	15.385	15.054	14.416
	60	0.182-0.183	14.770	14.465	13.589
	40	0.184-0.185	14.585	14.281	13.546
	20	0.189-0.190	15.041	14.741	14.237
Wind operation For DFIG	80	0.083-0.084	15.209	14.790	13.872
	60	0.122-0.123	13.979	13.538	12.932
	40	0.148-0.149	19.719	19.311	17.126
	20	0.158-0.159	20.265	19.920	17.769

2) Impact of Changing the Operating Conditions and DFIG Location: In this section, the influence of the different access locations of the integrated DFIG-based wind farm and changing the operating conditions on the effectiveness of the NPI is investigated. Accordingly, a 250-MW DFIG-based wind farm is integrated at bus 38, and it is replaced with SG9. In addition, to change the operating conditions, it is assumed that the system generation/load pattern is set to 88% level of the Base case operating condition. Accordingly, the corresponding operating point is obtained by running the power flow program and then TSA is performed. In this section, it is assumed that the fault occurs at bus 13 and is cleared by removing the line (13-14). To evaluate the effectiveness of the proposed approach, the NPI is used for TID and simulation results are compared to TSI and OOS.

According to the simulation result, the CCT obtained is 0.169–0.17 s. As Fig. 9 demonstrates, when the fault clearing time is 0.17 s, the grid is unstable and the NPI correctly recognizes the transient instability. Also, compared to the TSI and OOS, the NPI detects transient instability earlier than TSI by 1836 ms on average, and OOS by 1291 ms on average. As a result, the effectiveness of the NPI in a shorter time can also be approved here.

3) Discussion: Many studies have been conducted on transient stability analysis. Generally, it has been shown that Lyapunov's method based on TEF takes up 8% of material published about TSA [4]. Some conducted studies have been provided indices for TID that have been selected for the analysis and comparison in this section. The results of this comparison have been summarized in Table VI. Accordingly, the important points and characteristics of the proposed algorithm compared to other methods can be expressed as follows.

1) In this article, a two-axis model with the static excitation system is used for the SGs and the fifth-order model is

TABLE VI
COMPARISON OF THE PROPOSED ALGORITHM WITH PUBLISHED METHODS

Comparison Indicators	[9]	[10]	[13]	[18]	[21]	[29]	[30]	[31]	This paper
Model of SG / DFIG	C / N	T + E / -	N/-	C / N	T + E / F	T + E / F	T + E / F	C / N	T + E / F
Quantity used for TID	Rotor angle	KE	KE	Critical energy	KE	Rotor angle & velocity	Rotor angle & velocity	Inertia constant	KE + PEBS function
Ability to use PMU	✓	✓	✓	×	✓	✓	✓	✓	✓
Real-time application	✓	✓	✓	×	✓	✓	✓	✓	✓
Needless to estimate UEP	×	✓	×	×	✓	✓	✓	✓	✓
Effect of penetration of DFIG-based wind farm	×	×	×	✓	✓	×	×	✓	✓
Early detection time of proposed approach (ms)	101	23.1 BFC	200 AFC	N	165	491.11	491.87	N	1283.45
Effect of measurement error using PMUs	×	×	×	×	×	×	×	×	✓ SNR (60-100) dB

N = Not mentioned, C = Classic, T = Two axis, E = Excitation system, F = Fifth order, BFC = Before fault clearing, AFC = After fault clearing

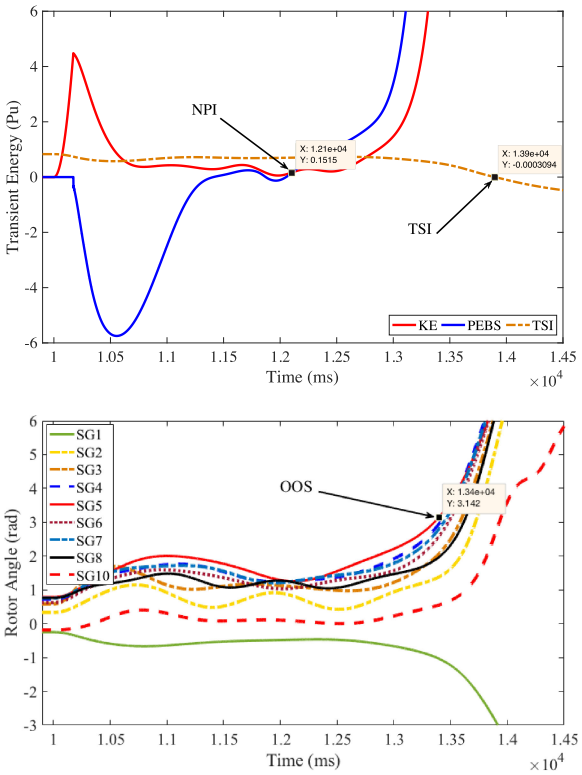

Fig. 9. KE, TSI, PEBS, and rotor angle of SGs in the unstable condition.

used for DFIG. Also, T-D simulation is used by the SI method.

2) In recent years, the use of the phasor measurement units (PMUs) has added new dimensions to wide-area measurements in the power systems [28]. The KE and the PEBS function in the postfault period are used in this article so that the required quantities can be easily measured by the PMU [8]. Therefore, the proposed algorithm is suitable for real-time applications.
3) The complexity and computational load of determining the UEP or the value of the critical energy, especially in multimachine power systems, is one of the most important problems in TID. In the proposed algorithm, considering the characteristics of the UEP, there is no need to calculate it directly for TID. However, in [9], [13], and [18], there was a need to calculate the UEP or the value of critical energy. In such conditions, the computational load increases, and the use of the method for the real-time applications is questioned.
4) All of the intelligent methods for TID are highly dependent on power system parameters and are not a general tool to be used in all grids with different parameters [13], whereas the proposed algorithm can be applied as a general tool to any power system with any change in topology and operating conditions.
5) In a stable condition, the minimum value of KE is very close to zero. However, the value of KE is not exactly zero in this state [8]. Accordingly, the assumption that the minimum KE is equal to zero in this state, which has been considered in some previous studies [10], is not accurate.
6) For the real-time validation of the scheme, the proposed method has been applied with consideration of the effect of measurement errors using PMUs. Accordingly, simulations were performed with consideration the signal-to-noise ratio (SNR) equal to 60–100 dB for two scenarios. It is shown that the measurement errors using PMUs have no significant effect on the proposed algorithm.
7) According to the simulation results in the 10-generator New England system case study, the NPI can generally detect accurately instability earlier than the OOS by 1283.45 ms on average.

In [21], only one simulation has been performed to show the effectiveness of the presented method in real-time applications,

in which the transient instability was detected earlier by 165 ms. Also, in studies [29] and [30], limited simulations have been represented that only analyze the status of the SG9. As can be observed, the early detection time of them has been obtained 491.11 and 491.87 ms on average, respectively.

In [32] is proposed that the maximum time, which the remedial actions are effective and can prevent the instability in the power system, be defined as the worst state. As this parameter varies for different networks, it must be calculated based on the simulation results. According to simulations on the 10-generator New England system, which is used as a benchmark, this time is calculated to equal to 800 ms for this network. Considering 200 ms for delay of receiving data from PMUs and sending the commands, 200 ms for the execution of remedial action scheme program the remaining time for execution of prediction program is 400 ms [32]. For the 10-generator New England system case study, as can be observed, the early detection time is more than 400 ms in all of the sections. Therefore, according to the simulation results, the effectiveness of the NPI for TID in a shorter time is approved for all states, and thus, adequate time for the remedial actions is available.

VI. Conclusion

This article presents a new index for TID by using the concept of the PEBS along with KE. In fact, the stable and unstable status is identified according to the behavior of KE and the PEBS function for postfault period and without directly calculating the UEP. The effectiveness of the proposed approach is evaluated in the WSCC 3-machine, 9-bus system, and the 10-generator New England system by simulating different scenarios. The sooner the transient instability is detected, the more time is left to take corrective and preventive measures to prevent total instability and blackouts in the power system.

According to the simulation results, in all studied cases of the 10-generator New England system, the NPI can detect accurately instability earlier than the OOS by 1283.45 ms on average. In this way, the effectiveness of the NPI for TID in a shorter time is approved for all states. Usage of the fundamental concepts, fast calculation, capability of the real-time application, and postfault data dependence are some advantages of the proposed approach.

References

[1] Global Wind Energy Council. 2021. [Online]. Available: https://gwec.net

[2] Y. Huang, W. Chen, X. Deng, J. Tang, G. Zhu, and H. Zhang, "Modelling of DFIG-based wind turbine for low-frequency oscillation analysis of power system with high penetration of distributed energy," in *Proc. 14th IET Int. Conf. AC DC Power Transmiss.*, Sep. 2018, pp. 2625–2628. [Online]. Available: https://ieeexplore.ieee.org/document/8694558

[3] N. Amjady and S. A. Banihashemi, "Transient stability prediction of power systems by a new synchronism status index and hybrid classifier," *IET Gener. Transmiss. Distrib.*, vol. 4, no. 4, pp. 509–518, Mar. 2010. [Online]. Available: https://ieeexplore.ieee.org/document/5427310

[4] A. R. Sobbouhia and A. Vahedi, "Transient stability prediction of power system: A review on methods, classification and considerations," *Elect. Power Syst. Res.*, vol. 190, Jan. 2021, Art. no. 106853. [Online]. Available: https://doi.org/10.1016/j.epsr.2020.106853

[5] R. Zhang, Y. Xu, Z. Y. Dong, and K. P. Wong, "Post-disturbance transient stability assessment of power systems by a self-adaptive intelligent system," *IET Gener. Transmiss. Distrib.*, vol. 9, no. 3, pp. 296–305, Feb. 2015. [Online]. Available: https://ieeexplore.ieee.org/document/7047332

[6] M. A. Chowdhurya, W. X. Shenb, N. Hosseinzadehc, and H. R. Potad, "A review on transient stability of DFIG integrated power system," *Int. J. Sustain. Eng.*, vol. 8, no. 6, pp. 405–416, Jun. 2015. [Online]. Available: https://doi.org/10.1080/19397038.2015.1050480

[7] J. C. Cepeda, J. L. Rueda, D. G. Colomé, and D. E. Echeverría, "Real-time transient stability assessment based on centre-of-inertia estimation from phasor measurement unit records," *IET Gener. Transmiss. Distrib.*, vol. 8, no. 8, pp. 1363–1376, Aug. 2015. [Online]. Available: https://doi.org/10.1049/iet-gtd.2013.0616

[8] S. Zhao, H. Jia, D. Fang, Y. Jiang, and X. Kong, "Criterion to evaluate power system online transient stability based on adjoint system energy function," *IET Gener. Transmiss. Distrib.*, vol. 9, no. 1, pp. 104–112, Jan. 2015. [Online]. Available: https://ieeexplore.ieee.org/document/7024960

[9] B. Alinezhad and H. K. Karegar, "Out-of-Step protection based on equal area criterion," *IEEE Trans. Power Syst.*, vol. 32, no. 2, pp. 968–977, Jun. 2016.

[10] M. Z. Jahromi and S. M. Kouhsari, "A novel recursive approach for real-time transient stability assessment based on corrected kinetic energy," *Appl. Soft Comput.*, vol. 48, pp. 660–671, Nov. 2016. [Online]. Available: https://doi.org/10.1016/j.asoc.2016.06.045

[11] E. Farantatos, R. Huang, G. J. Cokkinides, and A. P. Meliopoulos, "A predictive generator out-of-step protection and transient stability monitoring scheme enabled by a distributed dynamic state estimator," *IEEE Trans. Power Del.*, vol. 31, no. 4, pp. 1826–1835, Dec. 2015.

[12] D. Z. Fang, T. S. Chung, Y. Zhang, and W. Song, "Transient stability limit conditions analysis using a corrected transient energy function approach," *IEEE Trans. Power Syst.*, vol. 15, no. 2, pp. 804–810, May 2000.

[13] P. Bhui and N. Senroy, "Real-time prediction and control of transient stability using transient energy function," *IEEE Trans. Power Syst.*, vol. 32, no. 2, pp. 923–934, May 2016.

[14] J. G. Slootweg, S. W. H. de Haan, H. Polinder, and W. L. Kling, "General model for representing variable speed wind turbines in power system dynamics simulations," *IEEE Trans. Power Syst.*, vol. 18, no. 1, pp. 144–151, Feb. 2003.

[15] E. Muljadi, C. P. Butterfield, B. Parsons, and A. Ellis, "Effect of variable speed wind turbine generator on stability of a weak grid," *IEEE Trans. Energy Convers.*, vol. 22, no. 1, pp. 29–36, Feb. 2007.

[16] J. Liu *et al.*, "Impact of power grid strength and PLL parameters on stability of grid-connected DFIG wind farm," *IEEE Trans. Sustain. Energy*, vol. 11, no. 1, pp. 545–557, Feb. 2019.

[17] P. Ledesma and J. Usaola, "Doubly fed induction generator model for transient stability analysis," *IEEE Trans. Energy Convers.*, vol. 20, no. 2, pp. 388–397, May 2005.

[18] M. A. Chowdhurya, W. X. Shenb, N. Hosseinzadehc, and H. R. Potad, "Transient stability of power system integrated with doubly fed induction generator wind farms," *IET Renewable Power Gener.*, vol. 9, no. 2, pp. 184–194, Feb. 2015. [Online]. Available: https://doi.org/10.1049/iet-rpg.2014.0035

[19] M. A. Chowdhurya, W. X. Shenb, N. Hosseinzadehc, and H. R. Potad, "Quantitative assessment and comparison of fault responses for synchronous generator and wind turbine generators based on modified transient energy function," *IET Renewable Power Gener.*, vol. 8, no. 5, pp. 474–483, Jul. 2014. [Online]. Available: https://doi.org/10.1049/iet-rpg.2012.0323

[20] A. Mitra and D. Chatterjee, "A sensitivity based approach to assess the impacts of integration of variable speed wind farms on the transient stability of power systems," *Renewable Energy*, vol. 60, pp. 662–671, Dec. 2013. [Online]. Available: https://doi.org/10.1016/j.renene.2013.06.002

[21] M. Tajdinian, A. R. Seifi, and M. Allahbakhshi, "Transient stability of power grids comprising wind turbines: New formulation, implementation, and application in real-time assessment," *IEEE Syst. J.*, vol. 13, no. 1, pp. 894–905, May 2018.

[22] P. W. Sauer and M. A. Pai, *Power System Dynamics and Stability*. Upper Saddle River, NJ, USA: Prentice-Hall, 1998, pp. 149–153.

[23] A. Mitra and D. Chatterjee, "Active power control of DFIG-based wind farm for improvement of transient stability of power systems," *IEEE Trans. Power Syst.*, vol. 31, no. 1, pp. 82–93, Jan. 2016.

[24] M. V. A. Nunes, J. A. P. Lopes, H. H. Zurn, U. H. Bezerra, and R. G. Almeida, "Influence of the variable-speed wind generators in transient stability margin of the conventional generators integrated in electrical grids," *IEEE Trans. Energy Convers.*, vol. 19, no. 4, pp. 692–701, Nov. 2004.

[25] B. B. Adetokun, C. M. Muriithi, and J. O. Ojo, "Voltage stability assessment and enhancement of power grid with increasing wind energy penetration," *Int. J. Elect. Power Energy Syst.*, vol. 120, Sep. 2020, Art. no. 105988. [Online]. Available: https://doi.org/10.1016/j.ijepes.2020.105988
[26] M. Edrah, K. L. Lo, and O. Anaya-Lara, "Impacts of high penetration of DFIG wind turbines on rotor angle stability of power systems," *IEEE Trans. Sustain. Energy*, vol. 6, no. 3, pp. 759–766, Apr. 2015.
[27] F. Mei, "Small signal modeling and analysis of doubly fed induction generators in wind power applications," Ph.D. dissertation, Dept. Elect. Electron. Eng., Imperial College London, Univ. London, London, U.K., 2007.
[28] M. G. Adamiak *et al.*, "Wide area protection—Technology and infrastructures," *IEEE Trans. Power Del.*, vol. 21, no. 2, pp. 601–609, Mar. 2006.
[29] A. R. Sobbouhia and A. Vahedi, "Online synchronous generator out-of-step prediction by ellipse fitting on acceleration power—Speed deviation curve," *Int. J. Elect. Power Energy Syst.*, vol. 119, Jul. 2020, Art. no. 105965. [Online]. Available: https://doi.org/10.1016/j.ijepes.2020.105965
[30] A. R. Sobbouhia and A. Vahedi, "Online synchronous generator out-of-step prediction by electrical power curve fitting," *IET Renewable Power Gener.*, vol. 14, no. 7, pp. 1169–1176, Jan. 2020. [Online]. Available: https://doi.org/10.1049/iet-gtd.2018.5938
[31] Y. Zhang, J. Bank, E. Muljadi, Y. H. Wan, and D. Corbus, "Angle instability detection in power systems with high-wind penetration using synchrophasor measurements," *IEEE J. Emerg. Sel. Topics Power Electron.*, vol. 1, no. 4, pp. 306–314, Dec. 2013.
[32] H. Hosseini, S. Naderi, and S. Afsharnia, "New approach to transient stability prediction of power systems in wide area measurement systems based on multiple-criteria decision making theory," *IET Renewable Power Gener.*, vol. 13, no. 21, pp. 4960–4967, Sep. 2019. [Online]. Available: https://doi.org/10.1049/iet-gtd.2018.5313

Hamid Reza Shabani received the M.S. degree in power electrical engineering from Shahid Rajaee Teacher Training University, Tehran, Iran, in 2014. He is currently working toward the Ph.D. degree in electrical engineering with the Department of Electrical Engineering, Iran University of Science and Technology, Tehran, Iran.

His current project is evaluation of large-disturbance rotor angle instability in the modern power systems, with high penetration of wind power generation. His research interests include power system stability, power system dynamic and control, and renewable energy.

Mohsen Kalantar (Member, IEEE) received the Ph.D. degree from the Indian Institute of Technology Delhi, New Delhi, India, in 1991.

In 1992, he joined Iran University of Science and Technology (IUST), Tehran, Iran, as an Assistant Professor. Later, he was promoted to Full Professor in 2010. He is currently the Director of the Renewable Energy Research Laboratory, IUST. His research interests include renewable energy, distributed generation, and power system dynamic and control.

Amin Hajizadeh (Senior Member, IEEE) received the Ph.D. degree from K. N. Toosi University of Technology, Tehran, Iran, in 2010.

Since 2016, he has been an Associate Professor with the Department of Energy Technology, Aalborg University, Esbjerg, Denmark. His research interests include control of distributed energy resources and storage systems, control of power electronic converters for microgrid, and marine power systems.